

Pore Scale Spatial Analysis of Two Immiscible Fluids in Porous Media

HAIM GVIRTZMAN AND PAUL V. ROBERTS

Department of Civil Engineering, Stanford University, Stanford, California

A conceptual model is introduced describing the spatial distribution of two immiscible fluids in the pore space of sphere packings. The model is based on the ideal soil concept of homogeneous arrangement of identical spheres but is generalized to include random packing. It quantitatively analyzes the interfacial area between wetting and nonwetting fluids and between the fluids and the solid spheres, as a function of the saturation degree. These relationships depend on the packing arrangement of the spheres, the sphere radius, and the fluid-solid contact angle. The model focuses on the region of low saturation of the wetting phase, where the wetting phase is comprised of pendular rings. When the nonwetting phase appears as ganglia, the model assumes single-chamber ganglia. Three-dimensional graphical illustrations are provided. Three potential applications are pointed out: (1) to quantify the water-air interface in the unsaturated zone; (2) to analyze connate water interfacial area in petroleum reservoirs and to assess the effect of surfactants during enhanced oil recovery; and (3) to estimate the interface between groundwater and floating nonaqueous phase liquids above the water table.

INTRODUCTION

During the past two decades, increasing effort has been directed toward understanding and quantifying multiphase flow in porous media. The impetus for this research stems from the heightened awareness of groundwater contamination by organic liquids. This phenomenon has become a serious environmental threat and endangers public health. Groundwater contamination by synthetic organic chemicals was first reported in the literature almost 20 years ago [McKee *et al.*, 1972; Osgood, 1974]. Since then, most published reports have concentrated on the contaminant travel distances and dilution processes. Few studies examined the process of entrapment and/or mobilization of their residual saturation also [e.g., Roberts *et al.*, 1982; Kramer, 1982; Atwater, 1984; Villaume, 1985]. Concurrently, many theoretical and empirical models were developed. These models focus on describing the relative permeability of each of the immiscible fluids under the whole range of saturation [Williams and Wilder, 1971; Bear, 1972; Somers, 1974; Dullien, 1979]. Other models have concentrated on mass transfer between phases; i.e., dissolution, volatilization, and absorption [Van Der Waarden *et al.*, 1971; Pfannkuch, 1984; Roberts *et al.*, 1985; Hunt *et al.*, 1988a]. Several physically based mathematical models were established using different numerical codes [Faust, 1985; Pinder and Abriola, 1986; Corapcioglu and Baehr, 1987; Parker *et al.*, 1987; Delshad and Pope, 1989].

During the last decade, restoration of contaminated aquifers has become the most important topic and is currently undergoing intensive development [Thornton and Wootan, 1982; Wilson and Conrad, 1984; Hunt *et al.*, 1988b; Baehr *et al.*, 1989]. Practically, in most cases the pollution is removed by pumping, skimming, and ventilating. Recently, many researchers have been developing bioremediation strategies using microorganisms capable of degrading hydrocarbons

[Wilson and Wilson, 1985; McCarty, 1988; McCarty *et al.*, 1989].

It seems, however, that inadequate attention has been devoted to microscale (pore scale) investigation, particularly to the geometrical distribution of the immiscible fluids within the pores. The interfaces between phases play an important role in many processes, and thus analysis of their spatial configuration might contribute valuable information. The mass transfer during remediation acts, i.e., dissolution and volatilization, depends on the available surface area of the interfaces. Below a certain degree of residual saturation, the surface area might become a limiting factor. Also, bioremediation efficiency depends sometimes on the available surface area between aqueous and organic phases. The common hypothesis [Atlas, 1988] that degrading microorganisms position themselves on these interfaces, a position that assures them maximal access to both the hydrocarbon substrate and the water-soluble mineral nutrients, illustrates the importance of interfaces in these reactions. Moreover, the relative permeability of two fluid phases through porous media is affected by the fluid spatial distribution. Specifically, for multiphase flow it is necessary to consider not only the friction at the fixed solid-fluid boundaries, but also the friction at the dynamic fluid-fluid interfaces (each with its own friction properties), and perhaps also the fluid-fluid-solid junctions. In addition, in a more general perspective, basic properties related to the statics and dynamics of two fluid phases in porous media, such as wettability, capillarity, tortuosity, connectivity, and residual saturation, are best understood when described at the pore scale.

Microscale laboratory investigations have explored several features. Nuclear magnetic resonance (NMR) imaging has been used for the detection of entrapped air bubbles in porous media [Ronen *et al.*, 1986]. Optical microscopy has been used for the same purpose [Williams, 1966]. Scanning electron microscopy has been used to photograph water-air interfaces [Gvirtzman *et al.*, 1987] and to photograph residual oil ganglia [Chatzis *et al.*, 1983]. Important advances came from the use of network micromodels [Dullien, 1979]. The most comprehensive microscale laboratory investiga-

Copyright 1991 by the American Geophysical Union.

Paper number 91WR00303.
0043-1397/91/91WR-00303\$05.00

tion was done by *Schwille* [1988], who conducted flow visualization studies in two-dimensional packed glass beads using optical techniques. He simulated penetration, dispersion, and entrapment of both light and dense immiscible organic liquids into unsaturated and saturated porous media of different grain-size distributions. However, most of the observations were basically qualitative, and none of them has quantified the interfacial area between fluid phases.

This paper quantitatively describe the pore scale spatial distribution of two immiscible fluid phases according to the ideal soil model, i.e., packed beds made of homogeneous sphere grains. Further generalization, allowing different contact angles and random packing, is introduced. Additional explanations and illustrations are provided using newly developed, computerized graphical codes [*AutoCAD Release 10*, 1988]. The geometrical model will be introduced in the following section. It will be followed by a few examples and potential applications: (1) to quantify the water-air interface in the unsaturated zone; (2) to analyze connate water interface in petroleum reservoirs and estimate the effect of surfactants during enhanced oil recovery; and (3) to estimate the interface between groundwater and floating NAPLs above its water table.

CONCEPTUAL MODEL

Ideal Soil Model

No progress can be made in analyzing the geometrical structure of two fluid phases in porous media without a detailed description of the porous matrix. Pore space models provide a framework for such an analysis. The objective of these models is to provide a reasonable idealization of the geometrical structure of the prototype so that the desired characteristics can be treated mathematically. To this end, the model must incorporate the most relevant characteristics of the prototype, while its complexity should be kept at a manageable level. This approach is a complement to stochastic analyses.

Van Brakel [1975] summarized and classified almost all proposed pore space interconnectivity models. His review started with the simplest kinds of capillary tubes and ended with the most complicated three-dimensional, randomly arranged networks composed of tubes and junctions. Additional advanced and sophisticated networks were proposed later [*Koplik and Lasseter*, 1985; *Dias and Payatakes*, 1986]. However, most of these network models are unable to describe the complicated spatial distribution of two fluids in the three-dimensional pore space by simple physical considerations. Rather, they assume every element of the pore space to be either full or empty. Therefore in the present study the ideal soil model was adopted. This model is defined simply by regarding the solid matrix to be composed of perfectly spherical particles of identical size packed in several ordered ways. This conceptual model was originally introduced in the geology [*Graton and Fraser*, 1935], chemical engineering [*Haughey and Beveridge*, 1966], and soil science [*Haines*, 1930] literatures. In the present study this model is expanded and applied to cases where the void space contains two immiscible fluids. The criteria for describing the spatial distribution of fluids are based on wettability, surface tension and capillary pressure considerations. The interfacial areas between the two fluids as well as between each of them and the solid matrix are geometrically de-

scribed and calculated as a function of the sphere packing and the fluid saturation.

Model Versus Reality

Unfortunately, natural geological strata have porous structures that are much too complex for complete geometrical description. This is true even for the simpler porous media such as sand packs. Real porous media usually have a chaotic microstructure [*Chan et al.*, 1988]. Moreover, when applied for the description of transport dynamics, such as capillary rise, *Van Brakel* [1975] claimed that none of the existing pore space models can give even a qualitative description of any observed phenomena. Consequently, the advantage of using pore space models is doubtful.

On the other hand, the ideal soil concept provides a suitable model of porous media better than alternative models. *Rose* [1958] claimed that postulating spherical particles is a reasonable approximation of an unconsolidated or slightly consolidated sand aquifer. This is because of the high sphericity of most sand particles (due to weathering) as they occur in nature. Moreover, it is clear from considerations of random packing of oblate and prolate spheroids that the volume and surface area values are good approximations of those calculated for packing of the sphere system. Furthermore, we have generalized the Ideal Soil model to include random packing of spheres which spread over wide range of porosity values. It is obvious that such configurations are oversimplified, but they facilitate a study of the physical phenomena in multiphase systems. Although this ideal situation does not exist in nature, it provides a conceptual framework for analysis and illustrates basic relationships. Particularly, in our case, we use the pore space model only to describe the static configuration of the pore space fluids under steady state conditions, and we have not attempted to describe any transport phenomena.

Solid Matrix

Packing of spheres has two extreme cases: cubic packing (Figure 1a) is the most open one, with a calculated porosity of 0.4764, whereas rhombohedral packing (Figure 1b) is the tightest one, with a calculated porosity of 0.2595. The packing arrangement is usually defined by a "unit cell," which is the smallest portion of a body which gives complete representation of the manner of packing and of distribution of voids throughout the body [*Graton and Fraser*, 1935]. In our case the unit cell is a rhombohedron, characterized by the intersection angles σ between three orientations of sphere rows in space (angles at the edges of the rhombohedron). These angles are 90° and 60° in the cubic and rhombohedral packing (Figures 1c and 1d), respectively. Defining the sphere radius as R , the volume of a cubic unit cell is $8R^3$, and that of a rhombohedral unit cell is $4\sqrt{2}R^3$. The latter cell might be divided, for simplification, into one octahedron and two tetrahedra. *Mayer and Stowe* [1965] evaluated the porosity ε for the whole range of intermediate packing

$$\varepsilon = 1 - \frac{\pi}{6} (1 - 3 \cos^2 \sigma + 2 \cos^3 \sigma)^{-1/2}; \quad (1)$$

$$60^\circ \leq \sigma \leq 90^\circ$$

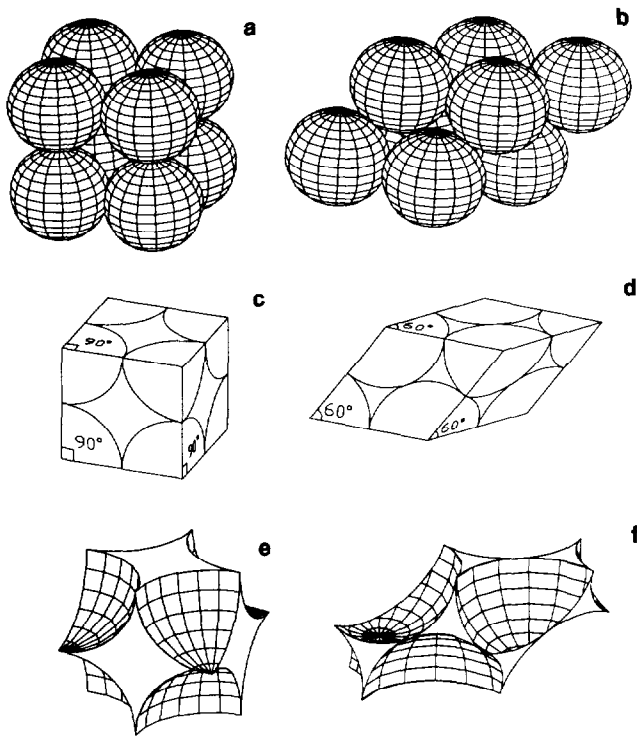


Fig. 1. (a) Cubic and (b) rhombohedral packings of identical spheres. The unit cells are defined by a rhombohedron with (c) $\sigma = 90^\circ$ and (d) $\sigma = 60^\circ$, respectively. The (e) and (f) unit voids for both packing arrangements are also shown (based on *Graton and Fraser [1935]*).

The "unit void" is the shape of the fluids contained in the interstitial space between the spheres in the unit cell. For a cubic packing there is only one type of pore space element; that is the void enclosed by eight spheres (Figure 1e). Under rhombohedral packing each unit void is built of one large pore element inside an octahedron, i.e., enclosed between six spheres, and two neighboring small pore elements inside tetrahedra, i.e., enclosed between four spheres (Figure 1f).

Fluid Spatial Distribution

Consider a case in which the wetted liquid is distributed homogeneously in the void space as pendular rings around tangent points of spheres. Figure 2 shows a pendular ring between two spheres and another one isolated from them. Liquid must accumulate in this configuration, under equilibrium conditions, because it requires minimum surface energy [*Smith, 1933*]. This situation is common in the unsaturated zone, where the pendular rings are the water, while the air fills the rest of the pore space [*Bear, 1972*]. Also, it is common for the connate water in petroleum and gas reservoirs [*Morrow and Heller, 1985*]. Clear photographs of such natural pendular rings were obtained by scanning electron microscope [*Gvirtzman et al., 1987, Figures 8 and 9*].

The relative size of pendular rings varies from zero, where only the nonwetting fluid fills the pores, up to the maximum size of pendular rings, where they meet each other. We define the pendular ring size using the angle φ , which is the angle between the lines connecting the centers of two neighboring spheres and the line from the sphere center to the edge of the ring (Figure 3). The angle φ varies in the

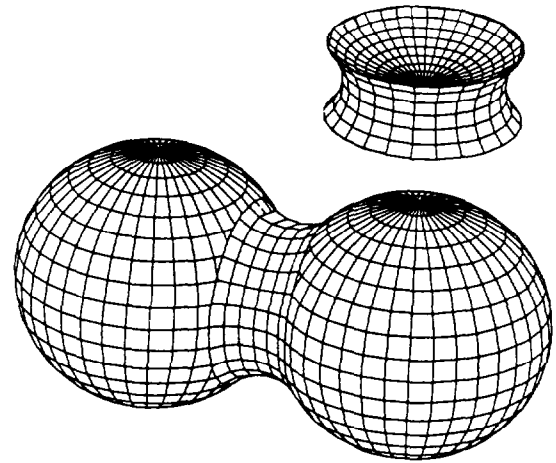


Fig. 2. A pendular ring between two spheres and another one isolated from the bounding solids.

range: $0 \leq \varphi \leq \sigma/2$. The geometrical structure of a pendular ring is described by the radii, r_1 and r_2 , of the curvatures formed by intersections of two perpendicular planes with the fluid interface (Figure 4). The pendular ring structure also depends on the contact angle of the liquid with the solid spheres ϑ . The capillary pressure at the interface can be calculated using the Laplace equation

$$P_c = \gamma_{wn} \left(-\frac{1}{r_1} + \frac{1}{r_2} \right) \cos \vartheta \tag{2}$$

where γ_{wn} is the interfacial tension between the wetting and the non-wetting fluids. Usually, the radius is positive when the center of the circle including the surface arc is in the liquid (r_2), and negative when in the atmosphere (r_1). Here we define both radii as positive numbers (to fit the geometrical figures). Therefore (2) was modified to include a minus sign before r_1 .

We recognize that in many cases the solid spheres are completely "coated" by a very thin water film, a few

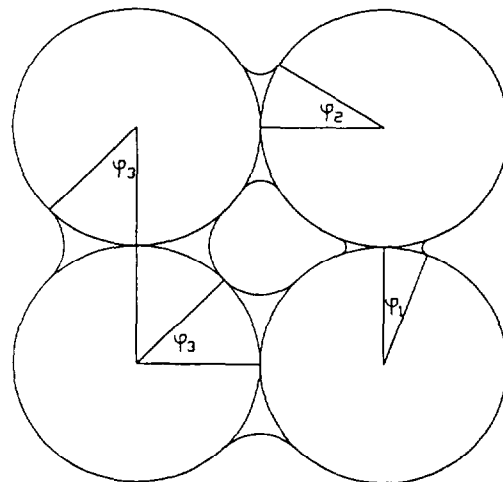


Fig. 3. A cross section through the centers of four spheres in a cubic pack arrangement, $\sigma = 90^\circ$. The pendular ring size of the wetting phase is defined by the angle φ . In this illustration: $\varphi_1 = 22^\circ$, $\varphi_2 = 32^\circ$, and $\varphi_3 = \sigma/2 = 45^\circ$ (where the pendular rings meet and merge).

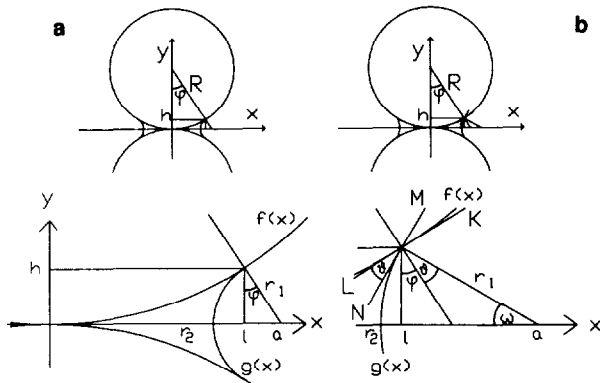


Fig. 4. Cross section through pendular ring for (a) $\vartheta = 0$ and (b) $\vartheta = 32^\circ$. Each of the two cross sections is enlarged below for detailed geometrical description. The radii r_1 and r_2 define the curvatures of the interface between the two fluids, and $f(x)$ and $g(x)$ are functions defining the circle and arc, respectively (see text and appendix).

molecules in thickness, due to the hydrophilic properties of the solid. However, we restrict our analysis to spheres whose radii are bigger than 10^{-3} mm; thus the coating water volume is negligible compared to the volume of water found in the form of rings in the grain contacts.

The geometrical analysis that follows provides the volumetric content of the wetting and nonwetting fluids and the specific surface area between the phases. The analysis is developed in the following steps: (1) A single pendular ring: identical spheres with zero contact angle, identical spheres with nonzero contact angle, and nonidentical spheres; and (2) a medium consisting of spheres containing many pendular rings: a regular packing and a random packing.

An Individual Pendular Ring

Assume two identical solid spheres tangent to each other, with a liquid pendular ring between defined by the angle φ . First, assume that the contact angle of the liquid with the solid is zero ($\vartheta = 0$). A cross section of these spheres passing through their centers is shown in Figure 4a. Restricting our analysis to sphere radii in the range of 1 mm to 10^{-3} mm, effects of gravity can be neglected because of the large magnitude of capillary forces in the small pores compared to the small potential energy difference between the top and bottom of a pore [Smith *et al.*, 1930; Melrose, 1966; Orr *et al.*, 1975]. Thus the interface between the fluids is assumed to have a constant curvature. The pendular ring is characterized by two radii: r_1 is the radius of the curvature whose center, a , is out of the liquid; and r_2 is the radius of the circle in a perpendicular plane whose center is in the liquid (at the tangent point between the two spheres). Therefore $a = r_1 + r_2$. The edge of the pendular ring, in Figure 4a, is the tangent point between the circles defined by R and r_1 . The basic trigonometric relations yield

$$r_1 = R \left[\frac{1 - \cos \varphi}{\cos \varphi} \right] \quad (3)$$

$$r_2 = R \left[\frac{\sin \varphi + \cos \varphi - 1}{\cos \varphi} \right] \quad (4)$$

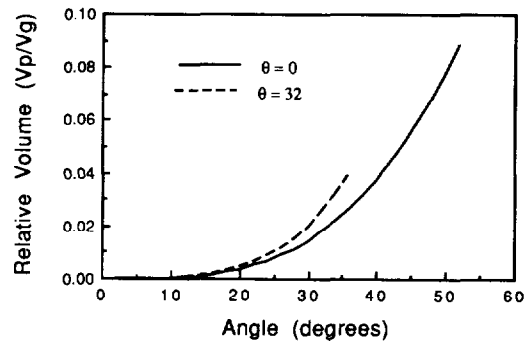


Fig. 5. Relative volume of an individual pendular ring vs. its size as expressed by the angle φ , for two possible contact angles ($\vartheta = 0$ and $\vartheta = 32^\circ$). The size of a pendular ring ranges from zero to φ_{\max} (which equals 53.1° and 37.1° , respectively).

Because the y axis is a symmetry axis (Figures 2 and 4), the pendular ring is really a solid of revolution and it is simple to calculate its volume and surface area. Its volume V_p and surface areas were formulated by Rose [1958]; details are given in the appendix;

$$V_p = 2\pi R^3 \left\{ 2 - 2 \cos \varphi - \tan \varphi \cdot \left[2 \sin \varphi - \tan \varphi + \left(\frac{\pi}{2} - \varphi \right) \left(\frac{\cos \varphi - 1}{\cos \varphi} \right) \right] \right\} \quad (5)$$

$$A_{wn} = 4\pi R^2 \left(\frac{1 - \cos \varphi}{\cos \varphi} \right) \left[\left(\frac{\pi}{2} - \varphi \right) \tan \varphi - (1 - \cos \varphi) \right] \quad (6)$$

$$A_{sw} = 4\pi R^2 (1 - \cos \varphi) \quad (7)$$

Figure 5 shows the ratio of the pendular ring volume V_p to a sphere volume V_g as a function of φ . The maximum size of a pendular ring is reached when the capillary force decreases to zero, i.e., when $r_1 = r_2$ (equation (2)). On the basis of (3) and (4), $\varphi_{\max} = 53.1^\circ$ as shown in Figure 5. Figure 6 shows the ratio of the interfacial area (A_{wn} and A_{sw}) of a pendular ring to a single grain surface area A_g .

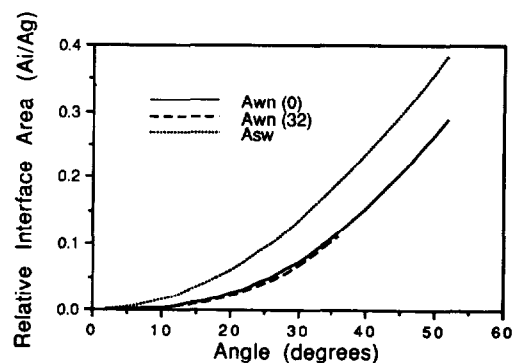


Fig. 6. Relative interfacial areas between phases of an individual pendular ring, A_{wn} and A_{sw} , versus its size as expressed by the angle φ , for two possible contact angles ($\vartheta = 0$ and $\vartheta = 32^\circ$).

Contact Angle Dependence

So far, the contact angle made between the solid surface and the fluid-fluid interface was assumed zero. However, in most cases the interface makes an angle ϑ with the solid surface (Figure 4b). Melrose [1965] developed a generalized formulation for the surface curvature and the resulting capillary pressure for this case but did not calculate the corresponding surface areas and volumes. Following is a generalized set of equations for the volume and interfacial area of a pendular ring for $\vartheta > 0$. Here the line MN is tangent to the arc whose radius is r_1 at the edge of the pendular ring, and the line KL is tangent to the sphere at that point. These two lines intersect at angle ϑ . The angle ω has to be introduced for this case (Figure 4b) and by geometrical considerations (with angles in radians)

$$\omega = \frac{\pi}{2} - \varphi - \vartheta \quad (8)$$

Using the law of sines in a triangle

$$\frac{\sin \frac{\pi}{2}}{r_1} = \frac{\sin \omega}{h} = \frac{\sin (\varphi + \vartheta)}{a - 1} \quad (9)$$

then the new radii are defined

$$r_1 = \frac{h}{\sin \omega} = R \left[\frac{1 - \cos \varphi}{\cos (\varphi + \vartheta)} \right] \quad (10)$$

$$r_2 = R \left[\sin \varphi - \frac{(1 - \cos \varphi)(1 - \sin (\varphi + \vartheta))}{\cos (\varphi + \vartheta)} \right] \quad (11)$$

The procedure for calculating the pendular ring's volume and interface areas is similar (see appendix)

$$V_p = 2\pi R^3 \left\{ (1 - \cos \varphi)^2 \left[1 - \cot \omega \left[\sin \varphi + \cot \omega \cdot \left(1 - \cos \varphi - \left(\frac{\sin \varphi}{\cos \omega} + \frac{1 - \cos \varphi}{\sin \omega} \right) \frac{\omega}{\cos \omega} \right) \right] \right] \right\} \quad (12)$$

$$A_{wn} = 4\pi R^2 \left(\frac{1 - \cos \varphi}{\sin \omega} \right) \cdot \{ \omega [(1 - \cos \varphi) \cot \omega + \sin \varphi] - (1 - \cos \varphi) \} \quad (13)$$

and A_{sw} is as in (7). Figures 5 and 6 shows the relative volume and interface area of a pendular ring for the example of $\vartheta = 32^\circ$. Under this situation, $\varphi_{\max} = 37.1^\circ$ (when $r_1 = r_2$). As is expected, for a given size of pendular ring as defined by the angle φ , the volume of a pendular ring with $\vartheta = 32^\circ$ is larger than that of $\vartheta = 0$, but its A_{wn} is smaller.

Nonidentical Spheres

More general equations for pendular rings between nonidentical spheres (where $\vartheta = 0$) were derived by Rose [1958]. For two spheres with radii R_1 and R_2 and a pendular ring characterized by the two respective angles φ_1 and φ_2 , it is possible to define r_3 , r_4 , and φ_3 using simple trigonometrical relationships (Figure 7):

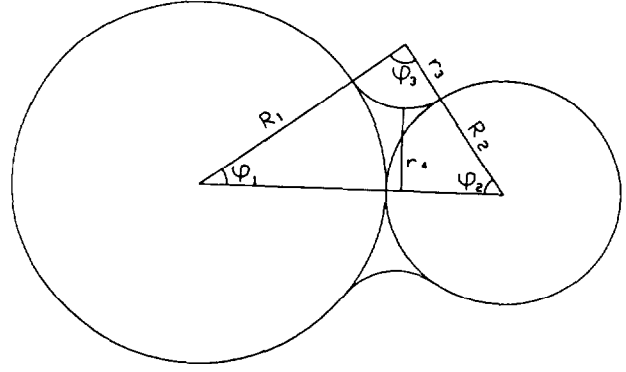


Fig. 7. A cross section through the center of a pendular ring between nonidentical spheres.

$$r_3 = \frac{R_1(R_1 + R_2)(1 - \cos \varphi_1)}{(R_2 - R_1) + (R_1 + R_2) \cos \varphi_1} \quad (14)$$

$$r_4 = (R_1 + r_3) \cos \varphi_1 - r_3 \quad (15)$$

$$\varphi_3 = \pi - \varphi_1 - \varphi_2 \quad (16)$$

On the basis of the above mentioned considerations the volume of this pendular ring is

$$V_p = 2\pi[A + B - C - D - E] \quad (17)$$

where

$$A = \frac{1}{6} (R_2 + r_3)^2 (R_1 + R_2) \sin^2 \varphi_2$$

$$B = \frac{2}{3} r_3^3 \sin \left(\frac{\varphi_3}{2} \right) \sin \left(\frac{\varphi_3}{2} + \varphi_2 \right)$$

$$C = \frac{2}{3} R_1^3 \sin^2 \left(\frac{\varphi_1}{2} \right)$$

$$D = \frac{2}{3} R_2^3 \sin \left(\frac{\varphi_2}{2} \right)$$

$$E = \frac{\varphi_3}{2} (R_2 + r_3) r_3^2 \sin \varphi_2$$

and its surface area is

$$A_{wn} = 2\pi \varphi_3 r_3 \cdot \left[(R_2 + r_3) \sin \varphi_2 - r_3 \sin \left(\frac{\varphi_3}{2} + \varphi_2 \right) \left(\frac{\sin \varphi_3 / 2}{\varphi_3 / 2} \right) \right] \quad (18)$$

Pendular Rings in a Regular Packed Medium

Figure 8 depicts the spatial distribution of a wetting phase in cubic and rhombohedral packings (Figures 8a and 8b), their unit cells (Figures 8c and 8d) and unit voids (Figures 8e and 8f). The volumetric content of each of the two fluids and their specific interfacial areas in the whole medium is calculated by extrapolation from a single pendular ring to a unit cell. During this extrapolation, one has to consider the

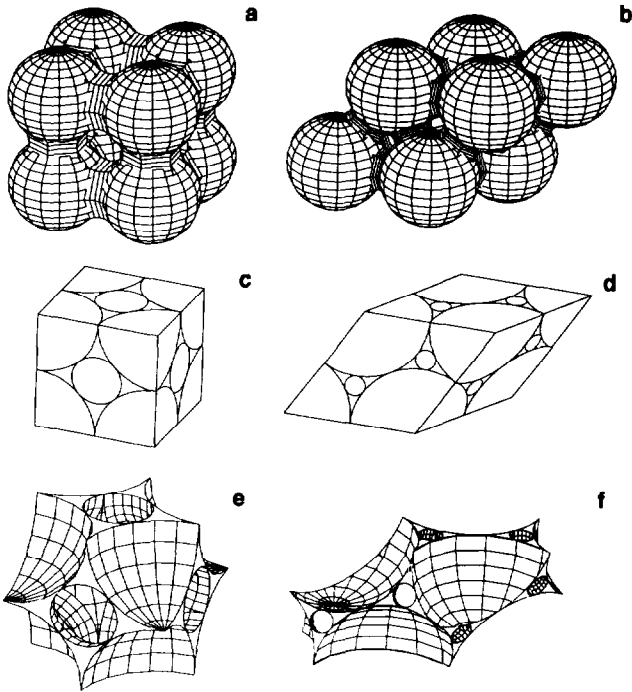


Fig. 8. (a) Cubic and (b) rhombohedral packings of identical spheres with wetting and nonwetting fluids filling the void space. (c) and (d) Unit cells and (e) and (f) unit voids for both packing arrangements are also shown. The pendular rings are drawn at their maximum size for a contact angle of zero.

number of pendular rings contained in a unit cell and the volume of the unit cell in each of the possible packing arrangements. The number of pendular rings depends on the number of spheres which each sphere touches, which is the "grain coordination number," n . For cubic packing, $n = 6$, and for rhombohedral packing, $n = 12$. A unit cell contains $n/2$ complete pendular rings, as each pendular ring belongs to two neighboring spheres. For example, cubic packing contains $n/2 = 3$ (i.e., 12 quarters in Figure 8c) pendular rings, and its volume is $8R^3$. Thus, when extrapolating from a single pendular ring to the whole medium, one has to multiply by the factor: $k_{\text{cubic}} = 3/8R^3$. A unit cell of rhombohedral packing, to use another example, contains $n/2 = 6$ pendular rings, as the cell consists of an octahedron and two tetrahedra. The octahedron contains 12 parts of a ring, where each part is $109.47^\circ/360^\circ$ and each tetrahedron contains six parts of a ring, where each part is $70.53^\circ/360^\circ$ (Figure 8d). The volume of a unit cell of rhombohedral packing is $4\sqrt{2}R^3$. Thus, when extrapolating from a single pendular ring to the whole medium, one has to multiply by the factor: $k_{\text{rhomb}} = 6/4\sqrt{2}R^3$. A general equation for extrapolation from a single pendular ring to a unit cell of identical spheres is

$$k = \frac{n/2}{\frac{4}{3}\pi R^3 \left(\frac{1}{1-\epsilon}\right)} = \frac{3n(1-\epsilon)}{8\pi R^3} \quad (19)$$

Therefore extrapolation of pendular ring volume and surface areas to the whole medium is calculated by

$$A_{\text{pack}} = k A_{\text{pendular}} \quad (20)$$

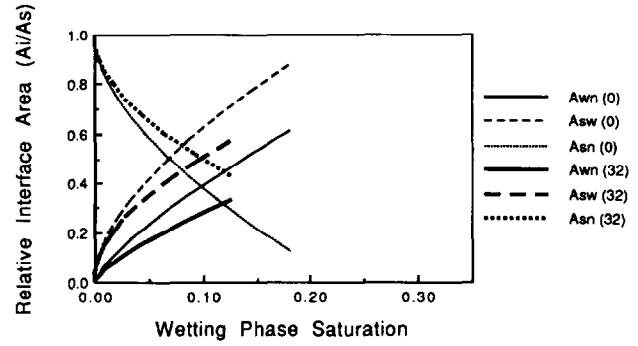


Fig. 9. Relative interfacial area between wetting (w), nonwetting (n), and solid (s) phases in a cubic packing of spheres as a function of the pendular ring saturation degree, for two possible contact angles. Maximum wetting phase saturation achieved when pendular rings merge or drain (see text).

$$V_{\text{pack}} = k V_{\text{pendular}} \quad (21)$$

On the basis of the above considerations, Figures 9 and 10 show the relative interfacial areas between the three phases for cubic and rhombohedral packing, respectively. The specific surface area of the solid spheres, A_s , is also differs between the two packing configurations (Figure 11).

An interesting phenomenon regarding the effect of the non-zero contact angle liquids is demonstrated in Figures 9 and 10. The maximum wetting phase saturation (at φ_{max}) under cubic packing is larger for perfectly wetting liquids ($\vartheta = 0$) than for intermediate wetting liquids ($\vartheta = 32^\circ$). For rhombohedral packing the opposite is true: namely, the saturation degree of a liquid with $\vartheta = 32^\circ$ is higher than with $\vartheta = 0$. The reason lies in the two opposing tendencies of partially wetting liquid ($\vartheta > 0$): the volume of such pendular ring is bigger for a given φ (Figure 5), but the capillary forces are smaller and the liquid drains under smaller φ_{max} . Therefore under cubic packing a wetting liquid with $\vartheta = 32^\circ$ will drain at $\varphi = 37.1^\circ$, making its maximum saturation only 13%, whereas a liquid with $\vartheta = 0$ achieves a maximum of 18% saturation (Figure 9). For rhombohedral packing the pendular rings merge at $\varphi = 30^\circ < \varphi_{\text{max}}$ and the pendular rings can not be drained ($C_p > 0$). Therefore the volume of a liquid with $\vartheta = 32^\circ$ achieves a maximum saturation of 34%, whereas a liquid with $\vartheta = 0$ achieves maximum saturation of only 24% (Figure 10).

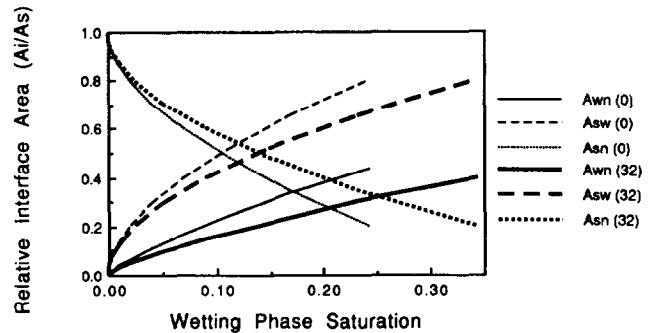


Fig. 10. Relative interfacial area between wetting (w), nonwetting (n), and solid (s) phases in a rhombohedral packing of spheres as a function of the pendular ring saturation degree, for two possible contact angles. Maximum wetting phase saturation achieved when pendular rings merge (see text).

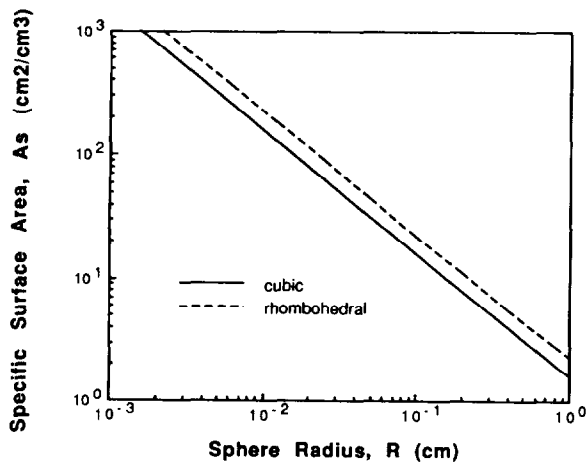


Fig. 11. Specific surface area of identical sphere packs as a function of the sphere radius for the two extreme cases of packing geometry: cubic and rhombohedral.

Random Packing

Random packing of identical spheres creates a mixed arrangement of pores with complicated geometries. The points of contact between a given sphere and adjacent spheres and their space distribution are complicated too. Random packing of spheres may create a wide range of porosity values. The relationship between porosity ϵ and the average grain coordination number n was discussed by *Haughy and Beveridge* [1969]. They compared theoretical relationships with experimental evidences. They reviewed four different empirical models describing the coordination number frequency distribution for randomly packed beds. We adopt their empirical relationship

$$n = 26.49 - \frac{10.73}{1 - \epsilon}; \quad 0.2595 \leq \epsilon \leq 0.4764 \quad (22)$$

that fits the two end points of cubic ($\epsilon = 0.4764$) and rhombohedral ($\epsilon = 0.2595$) packings, and shows nonlinear dependence between ϵ and n , as was found from experimental studies.

A random pack can also be approximated by an equivalent regular one. Three approaches were suggested for describing the equivalent medium. *Smith et al.* [1930] suggested considering the random-packed medium as a composition of two portions: cubic and rhombohedral chambers, homogeneously mixed together. They derived expressions for the porosity and equivalent coordination number as a function of the fraction of the two components. *Smith* [1932] also suggested another approach of considering the medium to be composed of only rhombohedral units, but with equidistant spacing between the spheres, adjusted to fit any given porosity. *Mayer and Stowe* [1965] suggested an equivalent medium by letting the edge angle of the unit cell, σ , vary in the range $60^\circ \leq \sigma \leq 90^\circ$.

Adopting the third approach, the interfacial areas between phases for a random packing of identical spheres can be estimated. A random packing with a porosity ϵ can be considered as equivalent to an effective packing of a theoretical rhombohedron with a specific edge angle σ , which can be evaluated using (1). The size of a single pendular ring then varies in the range $0 \leq \varphi \leq \sigma/2$. The grain coordination

number n of this packing can be estimated by (22). Extrapolation from a single pendular ring to the packed medium will be calculated by (19), (20), and (21). Now it is possible to plot the interface area between phases as a function of the wetting phase saturation degree for any given porosity of randomly packed spheres and for any given contact angle. However, the interface area function can not yet be approximated for a random pack of nonidentical spheres.

Nonwetting Phase Ganglion

Payatakes [1982] defined an oil ganglion as "a nodular blob of a non-wetting phase that occupies at least one and usually several adjoining chambers of the void space in a permeable medium." During its displacement a nonwetting phase loses its continuity and discrete ganglia are trapped and sometimes become immobile. When all openings between a void and its neighboring voids are closed by merging of pendular rings all around, a spherical ganglion is formed, and its radius can be as large as the maximum available radius. The assumption of ganglia distribution as discrete spherical droplets was adopted by several investigators [*Pfannkuch*, 1984; *DeZabala and Radke*, 1986; *Hunt et al.*, 1988a]. When a ganglion is composed of two or more contiguous chambers, each of the units will have a spherical structure except the side where two units are merged. At this contact point the nonwetting throat will be surrounded by pendular rings of the wetting phase. On the basis of the Percolation theory, *Larson et al.* [1977, 1981] have determined the statistical distribution of ganglia size and volume after the displacement of a nonwetting phase by a wetting phase. *Payatakes* [1982] stated that at the end of secondary oil recovery, residual oil exists in the form of discrete oil ganglia occupying 25–50% of the void space. Typically, oil ganglia at this stage have sizes ranging from one to fifteen elemental chamber volumes. On the basis of these simplifications the volumes and the interface areas of ganglia could be calculated in various packing arrangements. However, quantitative consideration of the geometry of ganglia is outside the scope of the present paper.

To extend the description of the interface area function to the region of high wetting-phase saturation, it is necessary to determine the ganglion configuration in the void cell. We will adopt the above mentioned, somewhat simplistic assumption, that the nonwetting phase is distributed in the pores only as single-chamber, spherical, isolated ganglia, whose radius varies between zero and the largest pore opening. The maximum possible radius of these ganglia can be $0.7321R$, $0.4142R$, and $0.2247R$, for cubic, octahedral and tetrahedral void cells, respectively. The curves shown in Figures 12 and 13 were derived by considering that a unit cell in a cubic packing contains one spherical ganglion, while a unit cell in a rhombohedral packing contains 3 spherical ganglia; i.e., one in an octahedral void and two in two neighboring tetrahedral voids.

Nevertheless, there is an intermediate range of saturation degrees which is uncovered. This range is between the stage where the wetting phase pendular rings meet each other and the stage where the non-wetting phase assumes the shape of isolated spherical ganglia surrounded by the wetting phase. This intermediate range is unstable and is affected by hydrostatic hysteresis. This type of hysteresis, which occurs within an individual pore space, was discussed by *Haines*

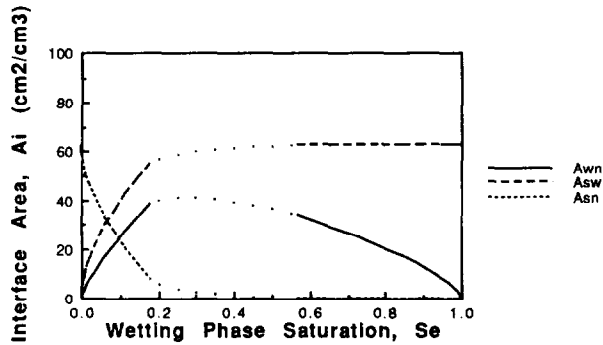


Fig. 12. Specific interfacial area between phases as a function of the wetting phase saturation under a cubic packing of 0.25-mm-radius spheres (for $\vartheta = 0$). The curves are determined for the pendular and insular stages but are estimated for the funicular stage due to hysteresis.

[1930] and *Smith* [1933]. There is a definite limited range of positions which a stable interface may occupy, and imbibition and drainage behave differently. For example, during drainage, when the non-wetting phase begins to enter a given pore, any advance in the interface is accompanied by an increase in capillary pressure. But if a point is reached where the advancing interface undergoes a decrease in curvature and hence in capillary pressure, such an interface is no longer configurationally stable. It "jumps" very rapidly, displacing the wetting phase from the pore. These jumps are usually called Haines jumps. The reverse situation is true for imbibition [*Melrose*, 1965]. The geometrical distribution of the two liquids is then complex, and the value of the interfacial area between the phases jumps between fixed upper and lower limits. Hence Figures 12 and 13 contain a undefined region, denoted by dotted lines.

POTENTIAL APPLICATIONS

Unsaturated Zone—Water and Air

Under equilibrium conditions, any pendular ring has fixed volume and interfacial areas, and the net mass transfer exchange across the interface is zero. The distribution of saturation of wetting liquid along a column of porous material varies with height. Three types of water saturation were defined by *Versluys* [1917], and accordingly, three zones along the unsaturated column were defined: pendular, funicular, and insular. The latter is known also as the capillary fringe zone. In the "pendular" zone at the upper part of the column the liquid is retained in isolated masses and each mass is a ring of liquid wrapped around the contact points of pairs of adjacent grains. Proceeding downward, the rings increase in size until they begin to coalesce and merge into more complicated masses, which is the "funicular" zone. Descending farther down the soil column, the more complicated liquid masses grow until finally a stage is reached where they merge and form a capillary surface which extends completely across the porous body; below this extends the "insular" zone which is the saturated part of the capillary fringe. In other words, in the pendular zone the wetting fluid is discontinuous while the nonwetting fluid is continuous. In the funicular zone, both fluids are essentially continuous. In the insular zone the wetting fluid is continuous while the nonwetting is discontinuous [*Bear*, 1979].

Smith [1933] claimed that, for uniform packed spheres, if a sufficiently long time has elapsed for achieving thermodynamic equilibrium, a balance will exist between gravity and capillary forces; the saturation distribution as a function of height can then be approximated by the Kelvin equation [*Thomson*, 1870]:

$$h = \frac{C_p}{\rho g} = \frac{\gamma}{\rho g} \left(\frac{1}{r_1} + \frac{1}{r_2} \right) \cos \vartheta \quad (23)$$

Equation (23) is only an approximation, as it ignores (1) deviation of gas from ideality, (2) deviation of liquid from incompressibility, and (3) deviation in vapor pressure distribution, [*Melrose*, 1966].

The individual isolated pendular rings will be "connected" to the bulk water phase by mass transfer via the vapor phase. If the curvatures of liquid masses at the same height above a free liquid are not equal, there will be evaporation from one and condensation onto the other until the curvatures become equal. The theoretical basis for this claim is that the well-known barometric formula (the relationship expressing the change of barometric pressure with elevation at constant temperature) may be applied to describe the vapor pressure distribution as a function of height above the free water surface. Figures 14 and 15 describe the distribution of C_p and A_i versus the saturation degree for the cubic and rhombohedral packings, respectively, under these circumstances.

Petroleum Reservoir—Water and Oil

Oil reservoirs form by accumulation of oil droplets, originating from source rocks, in geological traps during geological eras. The oil droplets tend to rise due to buoyancy forces and as oil accumulates in the trap, water is displaced. A substantial fraction of water, however, is found to remain along with the oil at heights well above the transition zone between the oil and its underlying aquifer [*Morrow and Heller*, 1985]. The vertical distribution of saturation degree along the transition zone fits the Kelvin distribution, as the geological time scale is long enough for achieving equilibrium conditions. The establishment of equilibrium depends on diffusional transport of dissolved water molecules through the oil phase. Figures 16 and 17 describe the distribution of C_p and A_i versus the water saturation degree

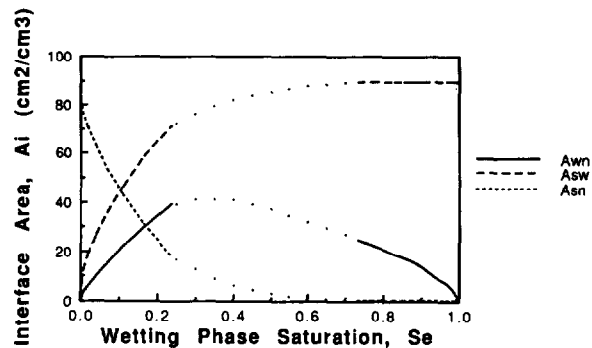


Fig. 13. Specific interfacial area between phases as a function of the wetting phase saturation under a rhombohedral packing of 0.25-mm-radius spheres (for $\vartheta = 0$). The curves are determined for the pendular and insular stages, but are estimated for the funicular stage due to hysteresis.

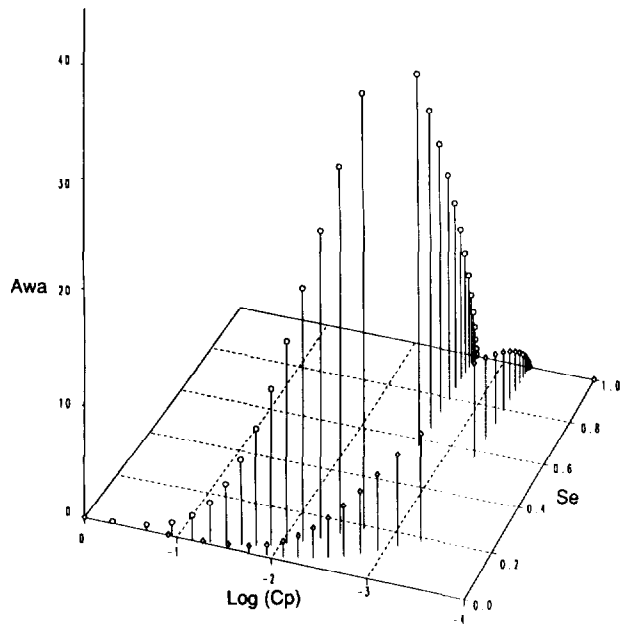


Fig. 14. Relation of water-air interfacial area (A_{wa}) to the retention curve function (C_p versus S_e) of a cubic packing of spheres with sphere radius of 0.25 mm (circles) and 1 mm (diamonds).

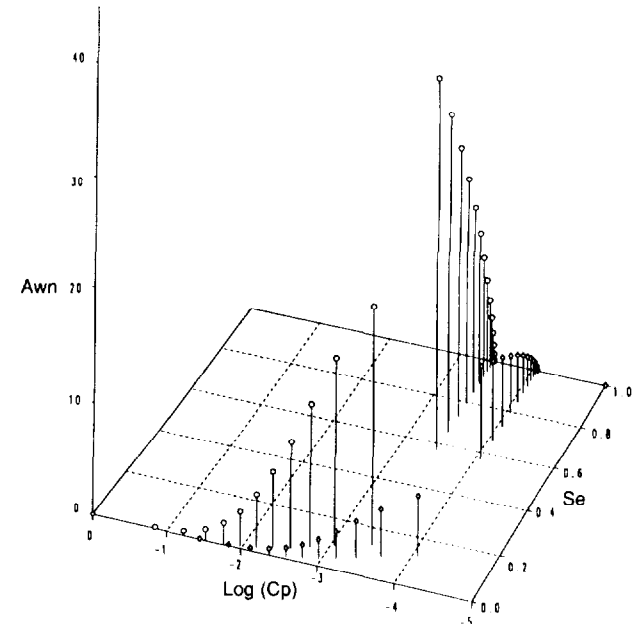


Fig. 16. Relation of water-oil interfacial area (A_{wn}) to the retention curve function (C_p versus S_e) of a cubic packing of spheres with sphere radius of 0.25 mm (circles) and 1 mm (diamonds). Contact angle of 32° and interfacial tension of 29.6 dynes/cm were used.

for the cubic and rhombohedral packings, respectively, with $\vartheta = 32^\circ$.

In enhanced oil recovery, surfactants are used to reduce the interfacial tension between oil and water [Morrow and Heller, 1985]. Moreover, the surfactants cause an increase of the contact angle ϑ and thus reduce the interface area between oil and water. This phenomenon is illustrated by our geometrical model. Figure 5 implies that for a given

volume of pendular ring, changing of the contact angle from $\vartheta = 0$ to $\vartheta = 32^\circ$ causes decrease of φ from 40° to 35° . Such a change is equivalent to the reducing of A_{wn} by about 25% (Figure 6). A better estimation can be obtained from Figures 9 and 10: Under cubic packing, for 12% saturation degree of connate water for example, changing the contact angle from $\vartheta = 0$ to $\vartheta = 32^\circ$ decreases A_{wn} by 25%. Under rhombohe-

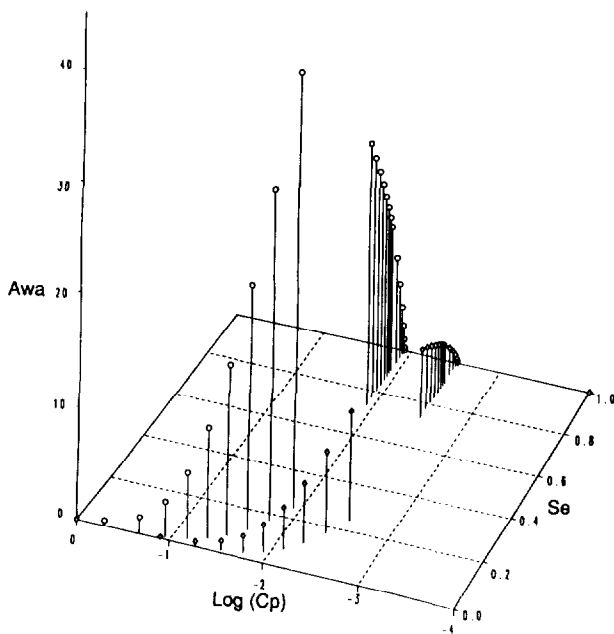


Fig. 15. Relation of water-air interfacial area (A_{wa}) to the retention curve function (C_p versus S_e) of a rhombohedral packing of spheres with sphere radius of 0.25 mm (circles) and 1 mm (diamonds).

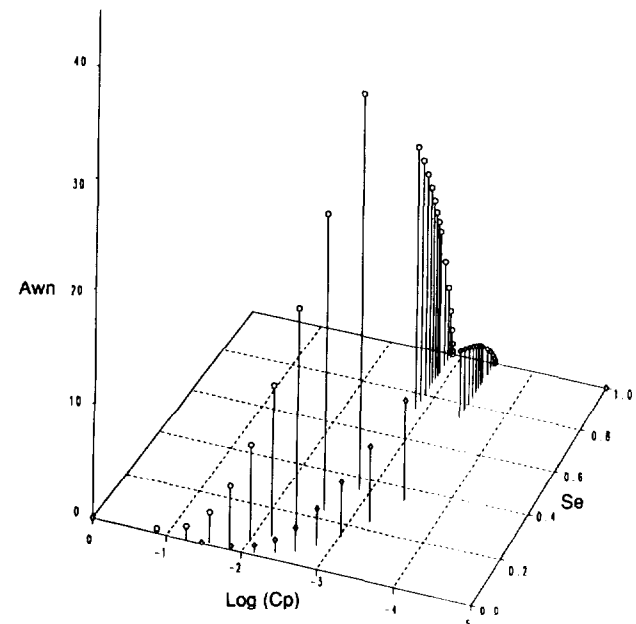


Fig. 17. Relation of water-oil interfacial area (A_{wn}) to the retention curve function (C_p versus S_e) of a rhombohedral packing of spheres with sphere radius of 0.25 mm (circles) and 1 mm (diamonds). Contact angle of 32° and interfacial tension of 29.6 dynes/cm were used.

dral packing, for 24% saturation of connate water, such a change causes decreases of A_{wn} by 30%. These principles can be applied to any particular case of random packing; only knowledge about the initial and final contact angles (before and after the addition of the surfactants) is necessary.

Floating NAPL Above Groundwater

Under nonequilibrium conditions, the volume of the pendular rings changes over time, owing to diffusional mass transfer between phases. The nonwetting ganglia are also subject to volume changes due to mass transfer, but they may also flow as distinct masses. Therefore the interface area between phases can be described as a function of the saturation degree, but not as a function of height above water table.

Such a case is common when groundwater is contaminated by NAPL [Hoag and Marley, 1986; Schwille, 1988]. When a mass of hydrocarbons or halogenated hydrocarbons enters into the subsurface as a result of a leak or spill, it mainly penetrates as a distinct phase through the unsaturated zone, partially dissolves into the soil moisture and partially evaporates in the aerated pores. When the capacity of the unsaturated zone is limited in relation to the organic liquid volume, it penetrates downward and reaches the water table. Organic liquids which are lighter than water will accumulate as a liquid lens floating above the water table [Osgood, 1974; Dowd, 1984]. However, halogenated organic liquids will penetrate downwards and might accumulate at the bottom of the aquifer [Villaume, 1985].

The interface between floating lens of organic liquid above the water table is similar to the natural transition zone between water and oil in a petroleum reservoir. The difference is in the temporal changes due to mass transfer by dissolution or by water table fluctuations. Therefore the interfacial areas between phases can be calculated for any given saturation degree based on Figures 9 and 10. The effectiveness of bioremediation actions depends among other parameters on the available surface area for bacterial activity, namely, the wetting-nonwetting interface. The maximum interface area between water and NAPL is achieved at about 30% water saturation, and it might be an additional parameter for choosing the optimum depth for stimulating biotransformation.

SUMMARY

A conceptual model is introduced describing the spatial distribution of two immiscible fluid phases in the pore space of sphere packings. The model is based on the ideal soil concept of homogeneous arrangement of identical spheres and is generalized to include random packing as well. The model describes the interfacial area between fluids and between the fluids and the solid spheres as a function of the wetting-phase saturation degree. This function depends on the sphere packing arrangement, the sphere radius and the fluid-solid contact angle. The model focuses on the pore scale, but is generalized to cover homogeneous media at larger scale. The model focuses on the region of low saturation, where the wetting phase is composed of pendular rings, but not when it appears as ganglia. The generality of this approach is limited by its reliance on the simplifying assumption of identical and spherical grains, which is uncommon in

nature. Nevertheless, it provides insight into the form and quantity of interfaces between fluids at the pore scale. Further research is needed for packs of nonidentical spheres.

Three potential applications of the model are discussed: (1) Quantitative analysis of the interface area between water and air in the unsaturated zone of phreatic aquifers. The interface areas are described in relation to the retention curve of the medium. (2) The interfaces between oil and connate water in petroleum reservoirs can be analyzed when the specific contact angle is given. Moreover, the model provides insight into the changing of the interfacial area when surfactants are applied during enhanced oil recovery. (3) When groundwater is contaminated by floating NAPLs, the interface area between the two liquids can be determined as a function of their partial saturation.

APPENDIX

The plane that is tangent to two adjacent spheres at their contact point divides the pendular ring into two identical halves. For the purpose of simplification, the following calculations deal only with one half. The coordinate system was chosen such that the origin is at the tangent point between the spheres, as seen in Figure 4a. The large circle of the sphere cross section, whose radius is R , is mathematically described by

$$x^2 + (y - R)^2 = R^2 \quad (\text{A1})$$

and the small circle of the pendular ring cross section, whose radius is r_1 , is described by

$$(x - a)^2 + y^2 = r_1^2 \quad (\text{A2})$$

where

$$a = r_1 + r_2 \quad (\text{A3})$$

The volume of a half pendular ring, which is a solid of revolution, can be calculated by integration using the method of cylindrical shells [Edwards and Penney, 1982]:

$$\frac{V_p}{2} = \int_0^1 2\pi x[f(x) - g(x)] dx \quad (\text{A4})$$

where

$$f(x) = y = \sqrt{R^2 - x^2} + R \quad (\text{A5})$$

$$g(x) = y = \sqrt{r_1^2 - (x - a)^2} \quad (\text{A6})$$

$$1 = R \sin \varphi \quad (\text{A7})$$

$$h = R(1 - \cos \varphi) \quad (\text{A8})$$

Substituting (A5) and (A6) into (A4), the volume of the whole pendular ring will be

$$V_p = 4\pi \int_0^1 x(\sqrt{R^2 - x^2} + R) dx - 4\pi \int_{r_2}^1 x\sqrt{r_1^2 - (x - a)^2} dx \quad (\text{A9})$$

which was analytically solved to be equal to

$$V_p = 2\pi R^3 \left\{ 2 - 2 \cos \varphi - \tan \varphi \left[2 \sin \varphi - \tan \varphi + \left(\frac{\pi}{2} - \varphi \right) \left(\frac{\cos \varphi - 1}{\cos \varphi} \right) \right] \right\} \quad (A10)$$

The interface between the two fluids is calculated by the method of revolving an arc about the axis lying in its plain, the y axis [Edwards and Penney, 1982]:

$$\frac{A_{wn}}{2} = \int_{r_2}^1 2\pi x \sqrt{1 + \left(\frac{dg}{dx} \right)^2} dx \quad (A11)$$

Substituting (A3) and (A6) into (A11) and differentiating

$$A_{wn} = 4\pi \int_{r_2}^1 x \sqrt{1 + \frac{(a-x)^2}{r_1^2 - (x-a)^2}} dx \quad (A12)$$

and it was analytically solved to be equal to

$$A_{wn} = 4\pi R^2 \left(\frac{1 - \cos \varphi}{\cos \varphi} \right) \left[\left(\frac{\pi}{2} - \varphi \right) \tan \varphi - (1 - \cos \varphi) \right] \quad (A13)$$

When the contact angle is not zero, as shown in Figure 4b ($\vartheta > 0$), then substituting (10) and (11) in (A9), in conjunction with (A3) and (A5)–(A7), the volume and interface area will be

$$V_p = 2\pi R^3 \left\{ (1 - \cos \varphi)^2 \left[1 - \cot \omega \left[\sin \varphi + \cot \omega \cdot \left(1 - \cos \varphi - \left(\frac{\sin \varphi}{\cos \omega} + \frac{1 - \cos \varphi}{\sin \omega} \right) \frac{\omega}{\cos \omega} \right) \right] \right] \right\} \quad (A14)$$

$$A_{wn} = 4\pi R^2 \left(\frac{1 - \cos \varphi}{\sin \omega} \right) \cdot \{ \omega [(1 - \cos \varphi) \cot \omega + \sin \varphi] - (1 - \cos \varphi) \} \quad (A15)$$

NOTATION

- a sum of curvature radii.
- A_g surface area of a single solid grain.
- A_s specific surface area of a solid pack.
- A_{sw} surface area between solid and wetting phases of a single pendular ring.
- A_{wn} surface area between wetting and non-wetting phases of a single pendular ring.
- A_{sn} surface area between solid and non-wetting phases of a single pendular ring.
- f(x) function of a circle defined by the principal cross section of a sphere.
- g(x) function of an arc defined by the principal cross section of a pendular ring.
- g gravitational acceleration.
- h axial height of a pendular ring.
- k extrapolation factor.
- l radial length of a pendular ring.
- n grain coordination number.

- P_c capillary pressure.
- r₁ radius of a curvature whose center is in the nonwetting phase.
- r₂ radius of a curvature whose center is in the wetting phase.
- R solid grain radius.
- S_e wetting-phase saturation fraction of total porosity.
- V_g volume of a single solid grain.
- V_p volume of a single pendular ring.
- x distance variable in horizontal direction.
- y distance variable in vertical direction.
- γ_{wn} interfacial tension between wetting and nonwetting fluids.
- ϑ solid-liquid contact angle.
- ρ water density.
- ε porosity.
- φ expansion angle of a pendular ring.
- φ_{max} maximum expansion angle of a pendular ring.
- σ angle of a rhombohedron edge.
- ω arc angle of a pendular ring (where ϑ > 0).

Acknowledgments. This research was conducted with the support of the Chaim Weizmann Fellowship Program, Israel, and the U.S. Environmental Protection Agency's Western Hazardous Substance Research Center (EPA R-815738).

REFERENCES

Atlas, R. M., Biodegradation of hydrocarbons in the environment, in *Environmental Biotechnology*, edited by G. S. Omenn, pp. 211–222, Plenum, New York, 1988.

Atwater, J. W., A case study of chemical spill: Polychlorinated biphenyls (PCBs) revisited, *Water Resour. Res.*, 20(2), 317–319, 1984.

AutoCAD Release 10, *Reference Manual*, 467 pp., Autodesk, 1988.

Baehr, A. L., G. E. Hoag, and M. C. Marley, Removing volatile contaminants from the unsaturated zone by inducing advective air-phase transport, *J. Contam. Hydrol.*, 4, 1–26, 1989.

Bear, J., *Dynamics of Fluids in Porous Media*, 764 pp., Elsevier, New York, 1972.

Bear, J., *Hydraulics of Groundwater*, 569 pp., McGraw-Hill, New York, 1979.

Chan, D. Y. C., B. D. Hughes, and L. Paterson, Fluid capacity distribution of random porous media, *Transp. Porous Media*, 3, 81–94, 1988.

Chatzis, I., N. R. Morrow, and H. T. Lin, Magnitude and detailed structure of residual oil saturation, *Soc. Petrol. Eng. J.*, 311–326, 1983.

Corapcioglu, M. U., and A. L. Baehr, A compositional multiphase model for groundwater contamination by petroleum products, 1, Theoretical considerations, *Water Resour. Res.*, 23(1), 191–200, 1987.

Delshad, M., and G. A. Pope, Comparison of three-phase oil relative permeability models, *Transp. Porous Media*, 4, 59–83, 1989.

DeZabala, E. F., and C. J. Radke, A non-equilibrium description of alkaline waterflooding, *SPE Reservoir Eng.*, 1(1), 29–43, 1986.

Dias, M. M., and A. C. Payatakes, Network models for two-phase in porous media, part 1, immiscible microdisplacement of non-wetting fluids, *J. Fluid Mech.*, 164, 305–336, 1986.

Dowd, R. M., Leaking underground storage tanks, *Environ. Sci. Technol.*, 18(10), 309, 1984.

Dullien, F. A. L., *Porous Media, Fluid Transport and Pore Structure*, 396 pp., Academic, San Diego, Calif., 1979.

Edwards, C. H. Jr., and D. E. Penney, *Calculus and Analytic Geometry*, pp. 239–288, chap. 5 Prentice Hall, Englewood Cliffs, N. J., 1982.

Faust, C. R., Transport of immiscible fluids within and below unsaturated zone: A numerical model, *Water Resour. Res.*, 21(4), 587–596, 1985.

Graton, S. C., and H. S. Fraser, Systematic packing of spheres with

- particular reference to porosity and permeability, *J. Geol.*, 43(8), 785-850, 1935.
- Gvirtzman, H., M. Magaritz, E. Klein, and A. Nadler, A scanning electron microscopy study of water in soil, *Transp. Porous Media*, 2, 83-93, 1987.
- Haines, W. B., Studies in the physical properties of soil, 5, The hysteresis effect in capillary properties and the modes of moisture distribution associated therewith, *J. Agric. Sci.*, 20, 97-116, 1930.
- Haughey, D. P., and G. S. G. Beveridge, Local voidage variation in a randomly packed bed of equal-sized spheres, *Chem. Eng. Sci.*, 21, 905-909, 1966.
- Haughey, D. P., and G. S. G. Beveridge, Structural properties of packed beds—Review, *Can. J. Chem. Eng.*, 47, 130-140, 1969.
- Hoag, G. E., and M. C. Marley, Gasoline residual saturation in unsaturated uniform aquifer materials, *J. Environ. Eng.*, 112(3), 586-604, 1986.
- Hunt, J. R., N. Sitar, and K. S. Udell, Nonaqueous phase liquid transport cleanup, 1, Analysis of mechanisms, *Water Resour. Res.*, 24(8), 1247-1258, 1988a.
- Hunt, J. R., N. Sitar, and K. S. Udell, Nonaqueous phase liquid transport and cleanup, 2, Experimental studies, *Water Resour. Res.*, 24(8), 1259-1269, 1988b.
- Koplik, J., and T. J. Lasseter, Two-phase flow in random network models of porous media, *Soc. Petrol. Eng. J.*, 89-100, 1985.
- Kramer, W. H., Groundwater pollution from gasoline, *Ground Water Monit. Rev.*, 2(2), 18-22, 1982.
- Larson, R. G., H. T. Davis, and L. E. Scriven, Percolation theory of residual phases in porous media, *Nature*, 268, 409-413, 1977.
- Larson, R. G., H. T. Davis, and L. E. Scriven, Displacement of residual nonwetting fluid from porous media, *Chem. Eng. Sci.*, 36, 75-85, 1981.
- Mayer, R. D., and R. A. Stowe, Mercury porosimetry: Break-through pressure for penetration between packed spheres, *J. Colloid. Sci.*, 20, 893-890, 1965.
- McCarty, P. L., Bioengineering issues related to in-situ remediation of contaminated soils and groundwater, in *Environmental Biotechnology*, edited by G. S. Omenn, pp. 143-162, Plenum, New York, 1988.
- McCarty, P. L., L. Semprini, and P. V. Roberts, Methodologies for evaluating the feasibility of in-situ biodegradation of halogenated aliphatic groundwater contaminants by methanotrophs, in *Hazardous Waste Treatment: Biosystem for Pollution Control*, pp. 69-82, Pittsburgh, Pa., 1989.
- McKee, J. E., F. B. Laverty, and R. M. Hertel, Gasoline in groundwater, *J. Water Pollut. Control Fed.*, 44(2), 293-302, 1972.
- Melrose, J. C., Wettability as related to capillary action in porous media, *Soc. Petrol. Eng. J.*, 5, 259-271, 1965.
- Melrose, J. C., Model calculations for capillary condensation, *Am. Inst. Chem. Eng. J.*, 12(5), 986-994, 1966.
- Morrow, N. R., and J. P. Heller, Fundamentals of enhanced recovery, in *Enhanced Oil Recovery, 1, Fundamentals and Analyses*, edited by E. C. Donaldson, G. V. Chilingarian, and T. Y. Yen, pp. 47-74, Elsevier, New York, 1985.
- Orr, F. M., L. E. Scriven, and A. P. Rivas, Pendular rings between solids: Meniscus properties and capillary force, *J. Fluid Mech.*, 67, 723-742, 1975.
- Osgood, J. O., Hydrocarbon dispersion in groundwater: Significance characteristics, *Ground Water*, 12(6), 427-436, 1974.
- Parker, J. C., R. J. Lenhard, and T. Kuppusamy, A parametric model for constitutive properties governing multiphase flow in porous media, *Water Resour. Res.*, 23(4), 618-624, 1987.
- Payatakes, A. C., Dynamics of oil ganglia during immiscible displacement in water-wet porous media, *Ann. Rev. Fluid Mech.*, 14, 365-393, 1982.
- Pfannkuch, H. O., Mass-exchange processes at the petroleum-water interface, *U.S. Geol. Surv. Water Resour. Invest.*, 84-4188, 23-48, 1984.
- Pinder, G. F., and L. M. Abriola, On the simulation of nonaqueous phase organic compounds in the subsurface, *Water Resour. Res.*, 22(9), 109S-119S, 1986.
- Roberts, J. R., J. A. Cherry, and P. W. Schwartz, A case study of a chemical spill: Polychlorinated biphenyls (PCBs), 1, History, distribution and surface translocation, *Water Resour. Res.*, 18(3), 525-534, 1982.
- Roberts, P. V., P. Cornel, and R. S. Summers, External mass transfer rate in fixed bed adsorption, *J. Environ. Eng.*, 111(6), 891-905, 1985.
- Ronen, D., M. Magaritz, N. Paldor, and Y. Bachmat, The behavior of groundwater in the vicinity of water table evidence by specific discharge profiles, *Water Resour. Res.*, 22, 1217-1224, 1986.
- Rose, W., Volumes and surface areas of pendular rings, *J. Appl. Physics*, 29(4), 687-691, 1958.
- Schwille, F. *Dense Chlorinated Solvents in Porous and Fractured Media*, 146 pp., Lewis, New York, 1988.
- Smith, W. O., Capillary flow through an ideal uniform soil, *Physics*, 3(3), 139-146, 1932.
- Smith, W. O., The final distribution of retained liquid in an ideal uniform soil, *Physics*, 4, 425-440, 1933.
- Smith, W. O., P. D. Foote, and P. F. Busang, Capillary retention of liquids in assemblages of homogeneous spheres, *Phys. Rev.*, 36, 524-530, 1930.
- Somers, J. A., The fate of spilled oil in the soil, *Hydrol. Sci. Bull.*, 19(4), 501-521, 1974.
- Thomson, W. (Lord Kelvin), On the equilibrium of vapor at curved surface of liquid, *Proc. R. Soc. Edinburg*, 7, 63-67, 1870.
- Thornton, J. S., and W. L. Wootan, Jr., Venting for the removal of hydrocarbon vapors from gasoline contaminated soil, *J. Environ. Sci. Health*, A17(1), 31-44, 1982.
- Van Brakel, J., Pore space models for transport phenomena in porous media, *Powder Technol.*, 11, 205-236, 1975.
- Van Der Waarden, M., A. L. A. M. Bridie, and W. M. Groenewoud, Transport of mineral oil components to groundwater, 1, Model experiments on the transfer of hydrocarbons from a residual oil zone to trickling water, *Water Resour.*, 5, 213-226, 1971.
- Versluys, J., Die Kapillaritaet der Boeden, *Inst. Mitt. F. Bodenk.*, 7, 117-140, 1917.
- Villaume, J. F., Investigations at sites contaminated with dense nonaqueous phase liquids (NAPLs), *Ground Water Monit. Rev.*, 5(2), 60-74, 1985.
- Williams, D. E., and D. G. Wilder, Gasoline pollution of groundwater reservoir—A case history, *Groundwater*, 9(6), 50-54, 1971.
- Williams, P. J., Movement of air through water in partly saturated soils, *Nature*, 212, 1463-1464, 1966.
- Wilson, J. L., and S. H. Conrad, Is physical displacement of residual hydrocarbons a realistic possible in aquifer restoration?, paper presented at Conference on Petroleum Hydrocarbons and Organic Chemicals in the Subsurface, National Well Water Association, Houston, Tex., 1984.
- Wilson, J. T., and B. H. Wilson, Biotransformation of trichloroethylene in soil, *Appl. Environ. Microbiol.*, 49(1), 242-243, 1985.

H. Gvirtzman and P. V. Roberts, Department of Civil Engineering, Stanford University, Stanford, CA 94305.

(Received December 29, 1989;
revised January 10, 1991;
accepted January 24, 1991.)